Available on CMS information server

CMS CR -2017/137

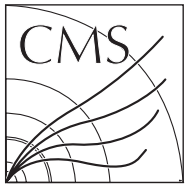

The Compact Muon Solenoid Experiment

Conference Report

Mailing address: CMS CERN, CH-1211 GENEVA 23, Switzerland

11 May 2017 (v2, 27 June 2017)

New CMS results from an angular analysis of B0- gt K*0,mu,mu decay studies

Mauro Dinardo for the CMS Collaboration

Abstract

First CMS measurement of the parameters P1 and P5 from B0- gt K*0, mu, mu decays.

Presented at *Moriond/EW2017 52nd Rencontres de Moriond on Electroweak Interactions and Unified Theories*

New CMS results on $B^0 \to K^{*0}\mu^+\mu^-$ decay studies

M. E. Dinardo on behalf of the CMS Collaboration
Università degli studi di Milano - Bicocca, Physics department,
3 Piazza della scienza, Milano - 20126, Italy

Angular distributions of the decay $B^0 \to K^{*0}\mu^+\mu^-$ are studied using data corresponding to an integrated luminosity of 20.5 fb^{-1} collected with the CMS detector at the LHC in proton-proton collisions at $\sqrt{s} = 8$ TeV. An angular analysis is performed, providing results for a number of physical observables, including P_5', which is of particular interest due to measurements from the LHCb Collaboration that exhibit potential discrepancy with the standard model. Based on a sample of 1397 signal events, the P_1 and P_5' angular parameters are determined as a function of the dimuon invariant mass squared. The measurement are in agreement with standard model predictions.

1 Introduction

Phenomena beyond the standard model (SM) of particle physics can become manifest directly, via the production of new particles, or indirectly, by affecting the production and decay properties of SM particles. Analyses of flavor-changing neutral current (FCNC) decays are particularly sensitive to the effects of new physics, since such decays are highly suppressed in the SM. An example is the decay $B^0 \to K^{*0}\mu^+\mu^-$, where K^{*0} indicates the $K^*(892)^0$ meson and where the charge conjugate reaction is implied unless otherwise stated. An angular analysis of this decay as a function of the dimuon invariant mass squared (q^2) allows its properties to be thoroughly investigated. While previous measurements of some of these variables by the BaBar, Belle, CDF, LHCb, and CMS experiments are consistent with the SM [1,2,3,4,5,6], the LHCb and Belle Collaborations recently reported a discrepancy larger than 3 standard deviations with respect to the SM for the so-called P_5' variable [7,8,9].

This Article presents a precise measurement of the P_5' variable, together with the P_1 variable, using a sample of $B^0 \to K^{*0}\mu^+\mu^-$ events collected in proton-proton (pp) collisions at center-of-mass energy $\sqrt{s} = 8$ TeV with the CMS detector at the CERN LHC. The data correspond to an integrated luminosity of 20.5 ± 0.5 fb^{-1}.

A detailed description of the CMS detector, together with a definition of the coordinate system used and the standard kinematic variables, can be found in Ref. [10,11].

2 Reconstruction, event selection, and efficiency

The criteria used to select the candidate events during data taking (trigger) and after full event reconstruction (offline) take advantage of the fact that B^0 mesons have relatively long lifetimes and therefore decay on average about 1 mm from their production point. The trigger only uses muons to select events, while the offline selection includes the full reconstruction of all decay products.

All events used in this analysis were recorded with the same trigger, requiring two identified muons of opposite charge to form a vertex that is displaced from the pp collision region (beamspot). The trigger required each muon to have $p_{\mathrm{T}} > 3.5$ GeV, $|\eta| < 2.2$, and to pass within 2 cm of the beam axis. The dimuon system was required to have $p_{\mathrm{T}} > 6.9$ GeV, a vertex fit χ^2 probability larger than 10%, and a separation of the vertex relative to the beamspot in the transverse plane of at least 3σ, where σ includes the calculated uncertainty in the vertex position and the measured size of the beamspot. In addition, the cosine of the angle, in the transverse plane, between the dimuon momentum vector and the vector from the beamspot to the dimuon vertex was required to be greater than 0.9.

The offline reconstruction requires at least two muons of opposite charge and two oppositely charged hadrons. The muons are required to match those that triggered the event readout, and also to pass general muon identification requirements. The dimuon system must satisfy the same requirements that were applied in the trigger.

The hadron tracks are required to fail the muon identification criteria, have $p_{\mathrm{T}} > 0.8$ GeV, and have an extrapolated distance d of closest approach to the beamspot in the transverse plane greater than twice the sum in quadrature of the uncertainty d and the beamspot transverse size. The invariant mass of the hadron pair must lie within 90 MeV of the nominal K^{*0} mass for either the $\mathrm{K}^+\pi^-$ or $\mathrm{K}^-\pi^+$ combination. To remove contamination from $\Phi \to \mathrm{K}^+\mathrm{K}^-$ decays, we temporarily assign the kaon mass to both charged hadrons, and then eliminate the event if the resulting invariant mass of the hadron pair is less than 1.035 GeV. The B^0 candidates are obtained by fitting the four charged tracks to a common vertex, and applying a vertex constraint to improve the resolution of the track parameters. The B^0 candidates must have $p_{\mathrm{T}} > 8$ GeV, $|\eta| < 2.2$, vertex fit χ^2 probability larger than 10%, vertex transverse separation S from the beamspot greater than 12 times the sum in quadrature of the uncertainty in S and the beamspot transverse size, and $\cos\alpha_{xy} > 0.9994$, where α_{xy} is the angle, in the transverse plane, between the B^0 momentum vector and the line-of-flight between the beamspot and the B^0 vertex. The invariant mass m of the B^0 candidate must lie within 280 MeV of the nominal B^0 mass (m_{B^0}) for either the $\mathrm{K}^-\pi^+\mu^+\mu^-$ or $\mathrm{K}^+\pi^-\mu^+\mu^-$ possibility. After applying the selection criteria, events in which at least one candidate is found contain on average 1.05 candidates. A single candidate is chosen based on the best B^0 vertex fit χ^2.

For the selected events, the dimuon invariant mass q and its uncertainty σ_q are calculated. We define $\mathrm{B}^0 \to \mathrm{J}/\psi\mathrm{K}^{*0}$ and $\mathrm{B}^0 \to \psi'\mathrm{K}^{*0}$ control samples through the requirements $|q - m_{\mathrm{J}/\psi}| < 3\sigma_q$ and $|q - m_{\psi'}| < 3\sigma_q$, respectively, where $m_{\mathrm{J}/\psi}$ and $m_{\psi'}$ are the nominal masses of the indicated meson. The average value of σ_q is about 26 MeV.

The remaining event sample still includes contributions from $\mathrm{B}^0 \to \mathrm{J}/\psi\mathrm{K}^{*0}$ and $\mathrm{B}^0 \to \psi'\mathrm{K}^{*0}$ decays, mainly due to unreconstructed soft photons in the charmonium decay. These events have a low q value and fall outside the sideband selection described above. These events also have a low reconstructed B^0 mass value (m) and can be selectively removed using a combined selection on q and m. For $q < m_{\mathrm{J}/\psi}$ ($q > m_{\mathrm{J}/\psi}$), we require $|(m - m_{B^0}) - (q - m_{\mathrm{J}/\psi})| > 160$ (60) MeV. For $q < m_{\psi'}$ ($q > m_{\psi'}$), we require $|(m - m_{B^0}) - (q - m_{\psi'})| > 60$ (30) MeV. After applying these requirements, 1397 events remain, which define the signal sample.

The four-track vertex candidate is identified as a B^0 or $\overline{\mathrm{B}}^0$ depending on whether the $\mathrm{K}^+\pi^-$ or $\mathrm{K}^-\pi^+$ invariant mass is closest to the nominal K^{*0} mass. The fraction of candidates assigned to the incorrect state is estimated from simulation to be 12–14%, depending on q^2.

The global efficiency, ϵ, is the product of the acceptance and the combined trigger, reconstruction, and selection efficiency, both of which are obtained from Monte Carlo (MC) simulation.

The acceptance is obtained from generated events, i.e. before the particle propagation with GEANT4, and is defined as the fraction of events with $p_{\rm T}({\rm B}^0) > 8$ GeV and $|\eta({\rm B}^0)| < 2.2$ that satisfy the single-muon requirement $p_{\rm T}(\mu) > 3.3$ GeV and $|\eta(\mu)| < 2.3$. These criteria are less restrictive than the final selection criteria, to account for finite detector resolution, because they are applied to generated quantities rather than to the reconstructed quantities. Only events passing the acceptance criteria are processed through the GEANT simulation, the trigger simulation, and the reconstruction software.

The combined trigger, reconstruction, and selection efficiency is given by the ratio of the number of events that pass the trigger and selection requirements and have a reconstructed $\rm B^0$ compatible with the generated $\rm B^0$ in the event, relative to the number of events that pass the acceptance criteria. Efficiencies are determined for both correctly tagged (the K and π have the correct charge) and mistagged (the K and π charges are reversed) candidates.

We search for possible backgrounds that peak at the $\rm B^0$ mass, mimicking signal, using simulation. The event selection is applied to inclusive samples of $\rm B^0 \to \psi(\mu^+\mu^-)X$, $\rm B_s \to \psi(\mu^+\mu^-)X$, $\rm B^+ \to \psi(\mu^+\mu^-)X$, and $\rm \Lambda_b \to \psi(\mu^+\mu^-)X$ events, where "X" represent a mixture of some of the most common decay modes with a $\rm J/\psi$ meson in the final state. No evidence for a peaking structure around the $\rm B^0$ mass is found. The distributions of the few events that satisfy the selection criteria mimic the combinatorial background shape. Studies of simulated $\rm B_s \to K^{*0}(K^+\pi^-)\mu^+\mu^-$ events, generated with the same branching fraction as $\rm B^0 \to K^{*0}(K^+\pi^-)$ $\mu^+\mu^-$ events, reveal that around 70 such events are expected to peak near the $\rm B_s$ mass, integrated over the entire q^2 signal region. This background is considered to be negligible in comparison to the 1397 signal events.

More details on the event reconstruction can be found in Ref. [6].

3 Analysis method

This analysis measures the P_1 and P_5' variables of the decay $\rm B^0 \to K^{*0}\mu^+\mu^-$ as a function of q^2. The decay is fully described as a function of the following angles: θ_ℓ the angle between the positive (negative) muon momentum and the direction opposite to the $\rm B^0$ ($\rm \overline{B}^0$) in the dimuon rest frame, $\theta_{\rm K}$ the angle between the kaon momentum and the direction opposite to the $\rm B^0$ ($\rm \overline{B}^0$) in the $\rm K^{*0}$ ($\rm \overline{K}^{*0}$) rest frame, and φ the angle between the plane containing the two muons and the plane containing the kaon and pion in the $\rm B^0$ rest frame. Although the $\rm K^+\pi^-$ invariant mass is required to be consistent with that of a $\rm K^{*0}$, there can be a contribution from spinless (S-wave) $\rm K^+\pi^-$ combinations. This is parametrized with three terms: $F_{\rm S}$, which is related to the S-wave fraction, and $A_{\rm S}$ and $A_{\rm S}^5$, which are the interference amplitudes between the S-wave and P-wave decays. Including these components, the angular distribution of $\rm B^0 \to K^{*0}\mu^+\mu^-$can be written as:

$$\begin{aligned}\frac{1}{{\rm d}\Gamma/{\rm d}q^2}\frac{{\rm d}^4\Gamma}{{\rm d}q^2{\rm d}\cos\theta_\ell{\rm d}\cos\theta_{\rm K}{\rm d}\varphi} = \quad & \frac{9}{8\pi}\left\{\frac{2}{3}\left[(F_{\rm S}+A_{\rm S}\cos\theta_{\rm K})\left(1-\cos^2\theta_\ell\right)+A_{\rm S}^5\sqrt{1-\cos^2\theta_{\rm K}}\right.\right. \\ & \left.\sqrt{1-\cos^2\theta_\ell}\cos\varphi\right]+(1-F_{\rm S})\left[2F_{\rm L}\cos^2\theta_{\rm K}\left(1-\cos^2\theta_\ell\right)\right. \\ & +\tfrac{1}{2}\left(1-F_{\rm L}\right)\left(1-\cos^2\theta_{\rm K}\right)\left(1+\cos^2\theta_\ell\right)+\tfrac{1}{2}P_1(1-F_{\rm L}) \\ & (1-\cos^2\theta_{\rm K})(1-\cos^2\theta_\ell)\cos 2\varphi+2P_5'\cos\theta_{\rm K}\sqrt{F_{\rm L}\left(1-F_{\rm L}\right)} \\ & \left.\left.\sqrt{1-\cos^2\theta_{\rm K}}\sqrt{1-\cos^2\theta_\ell}\cos\varphi\right]\right\}.\end{aligned} \tag{1}$$

The expression is an exact simplification of the full angular distribution, obtained by folding the φ and θ_ℓ angles about zero and $\pi/2$, respectively.

For each q^2 bin, the observables of interest are extracted from an unbinned extended maximum likelihood fit to four variables: the $\rm K^+\pi^-\mu^+\mu^-$ invariant mass m and the three angular

variables θ_ℓ, $\theta_{\rm K}$, and φ. For each q^2 bin, the unnormalized probability density function (pdf) has the following expression:

$$\begin{aligned}\mathrm{pdf}(m,\theta_{\rm K},\theta_\ell,\varphi) \quad &= Y_S^C\Big[S^C(m)\,S^a(\theta_{\rm K},\theta_\ell,\varphi)\,\epsilon^C(\theta_{\rm K},\theta_\ell,\varphi)\\ &+\tfrac{f^M}{1-f^M}\;S^M(m)\,S^a(-\theta_{\rm K},-\theta_\ell,\varphi)\,\epsilon^M(\theta_{\rm K},\theta_\ell,\varphi)\Big]\\ &+Y_B\,B^m(m)\,B^{\theta_{\rm K}}(\theta_{\rm K})\,B^{\theta_\ell}(\theta_\ell)\,B^{\varphi}(\varphi),\end{aligned} \tag{2}$$

where the contributions correspond to correctly tagged signal events, mistagged signal events, and background events. The parameters Y_S^C and Y_B are the yields of correctly tagged signal events and background events, respectively, and are determined in the fit. The parameter f^M is the fraction of signal events that are mistagged and is determined from MC simulation.

The signal mass probability functions $S^C(m)$ and $S^M(m)$ are each the sum of two Gaussian functions sharing the same mean, and describe the mass distribution for correctly tagged and mistagged signal events, respectively. In the fit, the mean, the four Gaussian σ parameters, and two fractions relating the contribution of each Gaussian, are determined from simulation. The function $S^a(\theta_{\rm K},\theta_\ell,\varphi)$ describes the signal in the three-dimensional (3D) space of the angular variables and corresponds to Eq. (1). The combination $B^m(m)\,B^{\theta_{\rm K}}(\theta_{\rm K})\,B^{\theta_\ell}(\theta_\ell)\,B^{\varphi}(\varphi)$ is obtained from $\rm B^0$ sideband data and describes the background in the space of $(m,\theta_{\rm K},\theta_\ell,\varphi)$, where $B^m(m)$ is an exponential function, $B^{\theta_{\rm K}}(\theta_{\rm K})$ and $B^{\theta_\ell}(\theta_\ell)$ are second- to fourth-order polynomials, depending on the q^2 bin, and $B^{\varphi}(\varphi)$ is a first-order polynomial.

The functions $\epsilon^C(\theta_{\rm K},\theta_\ell,\varphi)$ and $\epsilon^M(\theta_{\rm K},\theta_\ell,\varphi)$ are the efficiencies in the 3D space of $-1 \leq \cos\theta_{\rm K} \leq 1, 0 \leq \cos\theta_\ell \leq 1$, and $0 \leq \varphi \leq \pi$ for correctly tagged and mistagged signal events, respectively. The numerator and denominator of the efficiency are separately described with a nonparametric technique, which is implemented with a kernel density estimator.

The fit is performed in two steps. The initial fit uses sideband data in m to obtain the $B^m(m)$, $B^{\theta_{\rm K}}(\theta_{\rm K})$, $B^{\theta_\ell}(\theta_\ell)$, and $B^{\varphi}(\varphi)$ distributions (the signal component is absent from this fit). The sideband region is defined by $3\sigma_m < |m - m_{\rm B^0}| < 5.5\sigma_m$, where σ_m is the average mass resolution ($\approx$45 MeV) obtained from fitting a sum of two Gaussians with a common mean to simulated signal events. The distributions obtained in this step are then fixed for the second step, which is a fit to the data over the full mass range. The free parameters in this fit are the angular parameters P_1, P_5', and $A_{\rm S}^5$, and the yields Y_S^C and Y_B. To avoid difficulties in the convergence of the fit due to the limited number of events, the angular parameters $F_{\rm L}$, $F_{\rm S}$, and $A_{\rm S}$ are fixed to previous CMS measurements performed on the same data set with the same event selection criteria [6].

The expression describing the angular distribution of $\rm B^0 \to K^{*0}\mu^+\mu^-$, Eq. (1) and also its more general form in Ref. [13], can become negative for certain values of the angular parameters. In particular the pdf in Eq. (2) is only guaranteed to be nonnegative for a particular subset of the parameter space P_1, P_5', and $A_{\rm S}^5$, whose mathematical expression is nontrivial. The presence of such a physical region greatly complicates the numerical maximization process of the likelihood by MINUIT and especially the error determination by MINOS, in particular near the boundary between physical and unphysical regions. Therefore the second fit step is performed by discretizing the bidimensional space P_1 – P_5', and by maximizing the likelihood as a function of the nuisance parameters Y_S^C, Y_B, and $A_{\rm S}^5$ at fixed values of P_1 and P_5'. Finally the distribution of the likelihood values is fit with a bivariate Gaussian distribution whose position of the maximum inside the physical region corresponds to the best estimate of the angular parameters P_1 and P_5'.

The interference terms $A_{\rm S}$ and $A_{\rm S}^5$ must vanish if either of the two interfering components vanish. From Ref. [13], these constraints are implemented as $|A_{\rm S}| < \sqrt{12F_{\rm S}(1-F_{\rm S})F_{\rm L}}\,R$ and as $|A_{\rm S}^5| < \sqrt{3F_{\rm S}(1-F_{\rm S})(1-F_{\rm L})(1+P_1)}\,R$, where R is a ratio related to the S-wave and P-wave line shapes, estimated to be 0.89 near the $\rm K^{*0}$ mass. The constraint on $A_{\rm S}$ is naturally satisfied since the measurement of the parameters $F_{\rm S}$, $F_{\rm L}$, and $A_{\rm S}$ is taken from the previous

CMS analysis.

To ensure correct coverage for the uncertainties of the angular parameters, the Feldman-Cousins (FC) method is used with nuisance parameters. Two main sets of pseudo-experimental samples are generated to compute the coverage for the two angular observables P_1 and P_5'. The first (second) set, used to compute the coverage for P_1 (P_5'), is generated by assigning values to the other parameters as obtained by profiling the bivariate Gaussian distribution description of the likelihood determined from data at fixed P_1 (P_5') values. When fitting the pseudo-experimental samples, the same fit procedure as applied to data is used.

More details on the analysis method can be found in Ref. [6].

4 Systematic uncertainties

Since the efficiency is computed using simulation, extensive checks have been performed to verify the level of agreement between data and simulation. The systematic uncertainties associated with the efficiencies and other effects are described below and summarized in Table 1.

In the following we will discuss how the main contribution to the systematic uncertainty are determined, for an in-depth discussion cfr. [12].

Table 1: Systematic uncertainty contributions for the measurements of P_1 and P_5'. The total uncertainty in each q^2 bin is obtained by adding each contribution in quadrature. For each item, the range indicates the variation of the uncertainty in the q^2 bins.

Systematic uncertainty	$P_1(10^{-3})$	$P_5'(10^{-3})$
Simulation mismodeling	1–33	10–23
Fit bias	5–78	10–119
MC statistical uncertainty	29–73	31–112
Efficiency	17–100	5–65
Kπ mistagging	8–110	6–66
Background distribution	12–70	10–51
Mass distribution	12	19
Feed-through background	4–12	3–24
$F_{\rm L}$, $F_{\rm S}$, $A_{\rm S}$ uncertainty propagation	0–137	0–205
Angular resolution	2–68	0.1–12
Total systematic uncertainty	90–200	70–250

Because the efficiency functions are estimated from a finite number of simulated events, there is a corresponding statistical uncertainty in the efficiency. The efficiency functions are obtained from fits to simulated data. Alternatives to the default efficiency function are obtained by generating 100 new distributions, both for the numerator and the denominator of the efficiency ratio, using the default kernel density estimators as pdfs. The effect of these different efficiency functions on the final result is used to estimate the systematic uncertainty.

The principal check of the efficiency is obtained by comparing efficiency-corrected results obtained from the control channels with the corresponding world-average values. Since the $\rm B^0 \to J/\psi K^{*0}$ control channel has reduced uncertainties with respect to the $\rm B^0 \to \psi' K^{*0}$ channel, the efficiency as a function of the angular variables is checked by comparing the $F_{\rm L}$ measurements from the $\rm B^0 \to J/\psi K^{*0}$ channel, which contains 165 000 events. The resulting value of $F_{\rm L}$ is 0.537 ± 0.002(stat), compared with the world-average value of 0.571 ± 0.007(stat+syst). The difference of 0.034 is propagated to P_1 and P_5' by taking the RMS of their distributions resulting from refitting the data 200 times varying $F_{\rm L}$ within the discrepancy. As a cross check that this systematic uncertainty can be applied across all q^2 bins, the measured branching ratio, $\mathcal{B}(\rm B^0 \to \psi' K^{*0})\ \mathcal{B}(\rm B^0 \to J/\psi K^{*0}) = 0.479 \pm 0.008(\rm stat) \pm 0.055(R_\psi)$, is compared with the world-average value $0.484 \pm 0.018(\rm stat) \pm 0.011(\rm syst) \pm 0.012(R_\psi)$ and is seen to be in agreement

(R_φ refers to the branching ratio $\mathcal{B}(J/\psi \to \mu^+\mu^-)/\mathcal{B}(\psi' \to \mu^+\mu^-)$ where for the world-average is computed in the electron channel because of its smaller uncertainty).

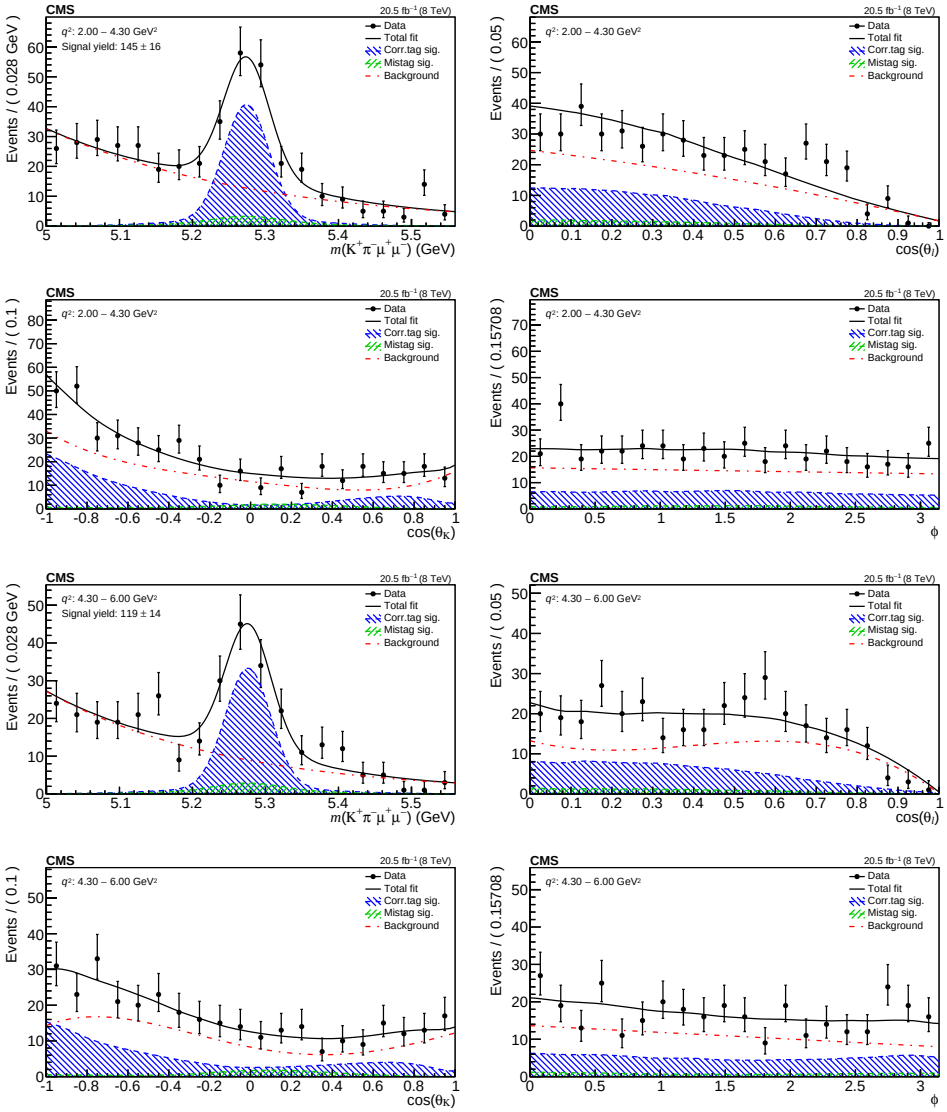

Figure 1 – $K^+\pi^-\mu^+\mu^-$ invariant mass and angular distributions for the second and third q^2 bin (top four plots) $2.00 < q^2 < 4.30$ GeV^2, and (bottom four plots) $4.30 < q^2 < 6.00$ GeV^2 [12]. Overlaid on each plot is the projection of the results for the total fit, as well as for the three components: correctly tagged signal, mistagged signal, and background. The vertical bars indicate the statistical uncertainties.

The pdf used in the analysis accommodates cases in which the kaon and pion charges are correctly or incorrectly assigned. Both of these contributions are treated as signal. The mistag fraction is fixed to the value obtained from MC simulation. In the statistically precise $B^0 \to J/\psi K^{*0}$ control channel, the mistag fraction is allowed to vary in the fit and a value of $f^M = (14.5 \pm 0.005)\%$ is found, to be compared to the simulated value of $(13.7 \pm 0.1)\%$. The 0.8% difference is propagated to P_1 and P_5' by taking the RMS of their distribution resulting from refitting the data 10 times varying f^M within this difference.

In the final fit, the F_L, F_S, and A_S parameters are fixed to values found in previous CMS measurements[6]. To propagate their uncertainty, 10 pseudo-experiments per q^2 bin are generated using the pdf parameters determined from the fit to data. The number of events in these pseudo-experiments is 100 times that of the data. The pseudo-experiments are then fitted twice, once with the same procedure as in data and once with all angular parameters free to vary. The

average ratio ρ of the statistical uncertainties in P_1 and P_5' determined from the two fits is used to compute the systematic uncertainty, which is proportional to the confidence interval determined with the FC method through the coefficient $\sqrt{\rho^2 - 1}$. The stability of ρ as a function of the number of events is also verified.

The systematic uncertainties are measured and applied in each q^2 bin, with the total systematic uncertainty obtained by adding the individual contributions in quadrature.

5 Results

The 1397 events of the signal event sample are fit in seven q^2 bins from 1 to 19 GeV^2. As an example, the individual mass and angular distributions for the second and third q^2 bins of the $K^+\pi^-\mu^+\mu^-$ channel, along with the fit projections, are shown in Fig. 1. The fitted values of the signal yields, P_1, and P_5', along with their associated uncertainties, are given for each of the q^2 regions in Table 2. These results are also shown in Fig. 2, along with the SM predictions. The fitted values for A_S^5 vary from -0.052 to $+0.057$.

Table 2: The measured signal yields, which include both correctly tagged and mistagged events, and the P_1 and P_5' values, in bins of q^2, for the decay $B^0 \to K^{*0}\mu^+\mu^-$. The first uncertainty is statistical and the second is systematic. The bin ranges are selected to allow comparisons to previous measurements.

q^2 (GeV^2)	Signal yield	P_1	P_5'
1.00–2.00	80 ± 12	$+0.12^{+0.46}_{-0.47} \pm 0.09$	$+0.10^{+0.32}_{-0.31} \pm 0.07$
2.00–4.30	145 ± 16	$-0.69^{+0.58}_{-0.27} \pm 0.09$	$-0.57^{+0.34}_{-0.31} \pm 0.11$
4.30–6.00	119 ± 14	$+0.53^{+0.24}_{-0.33} \pm 0.18$	$-0.96^{+0.22}_{-0.21} \pm 0.25$
6.00–8.68	247 ± 21	$-0.47^{+0.27}_{-0.23} \pm 0.15$	$-0.64^{+0.15}_{-0.19} \pm 0.13$
10.09–12.86	354 ± 23	$-0.53^{+0.20}_{-0.14} \pm 0.15$	$-0.69^{+0.11}_{-0.14} \pm 0.13$
14.18–16.00	213 ± 17	$-0.33^{+0.24}_{-0.23} \pm 0.20$	$-0.66^{+0.13}_{-0.20} \pm 0.18$
16.00–19.00	239 ± 19	$-0.53^{+0.19}_{-0.19} \pm 0.16$	$-0.56^{+0.12}_{-0.12} \pm 0.07$

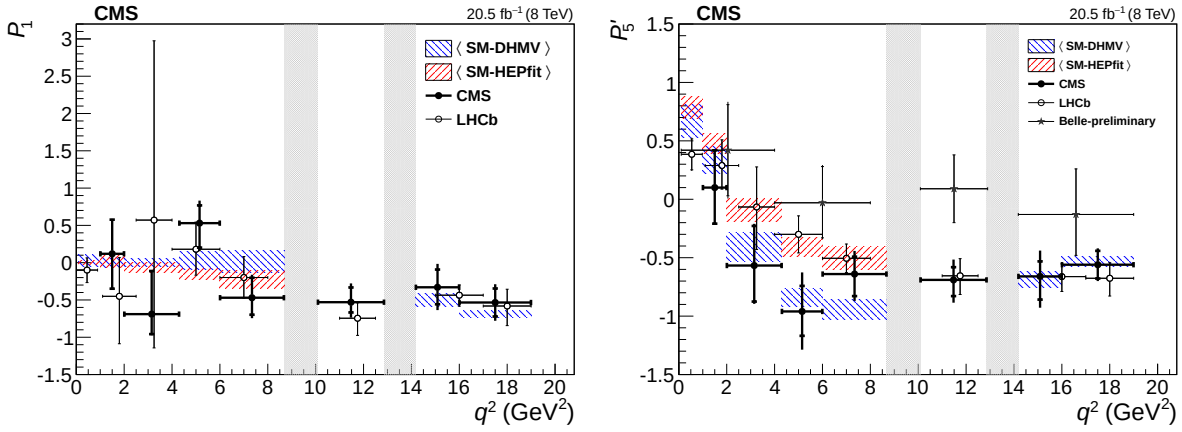

Figure 2 – Measured values of P_1 and P_5' versus q^2 for $B^0 \to K^{*0}\mu^+\mu^-$ from CMS [12], compared with LHCb [7] and Belle [9] results. The statistical uncertainty is shown by the inner vertical bars, while the outer vertical bars give the total uncertainty. The horizontal bars show the bin widths. The vertical shaded regions correspond to the J/ψ and ψ' resonances. The red and blue hatched regions show two SM predictions averaging over each q^2 bin to provide a direct comparison to the data. Reliable theoretical predictions are not available near the J/ψ and ψ' resonances.

Two SM predictions, SM-DHMV and SM-HEPfit, are available for comparison with the measured angular parameters. The SM-DHMV result, derived from Refs. [14,13], updates the calculations from Ref. [17] to account for the known correlation between the different form factors [18].

Light-cone sum rule predictions, which are valid in the low-q^2 region, are also combined with lattice determinations at high q^2 [19] to yield more precise determinations of the form factors over the full q^2 range. The hadronic charm-loop contribution is derived from Ref. [20]. The SM-HEPfit result, derived from the calculation reported in Refs. [15,16], uses full QCD form factors [18] and derives the hadronic contribution from LHCb data [7]. Reliable theoretical predictions are not available near the J/ψ and ψ' resonances. The two SM predictions are shown in comparison to the data in Fig. 2. Both are seen to be in agreement with the CMS results, although the agreement with SM-DHMV is somewhat better. Thus we do not obtain evidence for physics beyond the SM. Qualitatively, the LHCb data appear to be in better agreement with the SM-HEPfit prediction than with SM-DHMV result, but the uncertainties are too large to allow a definite conclusion.

6 Summary

Using pp collision data recorded at $\sqrt{s} = 8$ TeV with the CMS detector at the LHC, corresponding to an integrated luminosity of 20.5 fb^{-1}, an angular analysis has been performed for the decay $B^0 \to K^{*0}\mu^+\mu^-$. In total, 1397 signal events are obtained. For each bin of the dimuon invariant mass squared (q^2), unbinned maximum likelihood fits are performed to the distributions of the $K^+\pi^-\mu^+\mu^-$ invariant mass and three decay angles, to obtain values of the P_1 and P_5' parameters. The results are among the most precise to date and are consistent with standard model predictions and previous measurements.

References

1. BaBar Collaboration, *Phys. Rev.* D **79**, 031102 (2009)
2. Belle Collaboration, *Phys. Rev. Lett.* **103**, 171801 (2009)
3. CDF Collaboration, *Phys. Rev. Lett.* **108**, 081807 (2012)
4. LHCb Collaboration, *JHEP* **08**, 131 (2013)
5. CMS Collaboration, *Phys. Lett.* B **727**, 77 (2013)
6. CMS Collaboration, *Phys. Lett.* B **753**, 424 (2016)
7. LHCb Collaboration *JHEP* **02**, 104 (216)
8. S. Descotes-Genon, J. Matias, and J. Virto, *JHEP* **06**, 092 (2016)
9. Belle Collaboration, *Phys. Rev. Lett.* **118**, 111801 (2017)
10. CMS Collaboration, *JINST* **3**, S08004 (2008)
11. CMS Collaboration, *JINST* **9**, P10009 (2014)
12. CMS Collaboration, *CMS PAS BPH* **008** (2015)
13. S. Descotes-Genon, T. Hurth, J. Matias, and J. Virto, *JHEP* **05**, 137 (2013)
14. S. Descotes-Genon, J. Matias, M. Ramon, and J. Virto, *JHEP* **01**, 048 (2013)
15. M. Ciuchini, M. Fedele, E. Franco, S. Mishima, A. Paul, L. Silvestrini, M. Valli, *JHEP* **06**, 116 (2016)
16. M. Ciuchini, M. Fedele, E. Franco, S. Mishima, A. Paul, L. Silvestrini, M. Valli, *arXiv*:1611.04338
17. P. Ball and R. Zwicky, *Phys. Rev.* D **71**, 014029 (2005)
18. A. Bharucha, D. M. Straub, and R. Zwicky, *JHEP* **08**, 098 (2016)
19. R. R. Horgan, Z. Liu, S. Meinel, and M. Wingate, *Phys. Rev.* D **89**, 094501 (2014)
20. A. Khodjamirian, T. Mannel, A. A. Pivovarov, and Y.-M. Wang, *JHEP* **09**, 089 (2010)